JSEE Vol. 24, No. 1&2, 2022 DOI: 10.48303/jsee.2023.2000758.1057

Research Paper

Crustal Structure of the Northern Lut Block in Eastern Iran Using P Wave Receiver Function Migration

Azar Afshar[1], Meysam Mahmoodabadi[2], Farzam Yaminifard[3*] and Gholam Javan-Doloei[3]

1. Ph.D. Student, International Institute of Earthquake Engineering and Seismology (IIEES), Tehran, Iran
2. Assistant Professor, Seismological Research Center, International Institute of Earthquake Engineering and Seismology (IIEES), Tehran, Iran
3. Associate Professor, Seismological Research Center, International Institute of Earthquake Engineering and Seismology (IIEES), Tehran, Iran,
*Corresponding Author; email: faryam@iiees.ac.ir

Received: 24/04/2023
Revised: 12/05/2023
Accepted: 15/05/2023

ABSTRACT

To investigate the crustal structure of the northeast of Lut block and Eastern Iranian Ranges, we deployed 31 seismic stations along a 230 km profile for a period of approximately nine months. Using the migration of P-wave receiver functions, we analyzed changes in the Moho depth along this profile. Our results indicate that the boundary between the crust and upper mantle is nearly flat, with a depth of approximately 40 km. Furthermore, we found that the thickness of the crust is relatively high beneath the Lut-Afghan Block boundaries and Bagheran Mountain, where receiver functions suggest the presence of more complex structures including inclined interfaces. Our findings suggest that the collision of Lut-Afghan blocks has not significantly increased the crustal thickness in the northeast Iran compared to the Zagros collision zone in the southwest of Iran. Rather, we propose that the observed shortening in this region is primarily due to the interaction of strike-slip motions, which can accommodate shortening through mechanisms such as rotation and wedge escaping.

Keywords:
Crust; Lut Block; Moho; Receiver function

1. Introduction

The eastern part of Iran is a long north-south belt, which is mainly composed of rocks of Cenozoic age and extends between the Afghan Block in the east and Lut Block in the west (Stocklin, 1968). The geological evolution of the eastern Iran can be attributed to multiple factors, including the convergence of the Arabian and Indian plates with Eurasia, the escape of the Afghan Block towards Iran, the subduction of Makran, the evolution of the Sistan Ocean, and igneous activities (Berberian & King, 1981; Walker & Jackson, 2004; Walpersdorf et al., 2014; Bagheri & Stampfli, 2008; Hollingsworth et al., 2010; Allen et al., 2011; Nozaem et al., 2013; Bagheri & Damani Gol, 2020). Together, these complex interactions have shaped the geological and tectonic features of the region, contributing to its unique and diverse characteristics. The geodynamics of eastern Iran area has received attention in recent years, and considering the limitations in geological and geochemical studies and inconsistency of their results in this region, studying the structure of lithosphere in this region using seismological methods can help understanding of its geological evolution. For this

purpose, Teleseismic seismograms, at epicentral distance of 30 to 90 degrees and with a magnitude greater than 5.5, recorded by 31 temporary and permanent seismic stations, are used to study the structure of the crust and the upper mantle of the Eastern Iran in the South Khorasan province, along a 230 km profile oriented N40°E.

In this study, P-wave receiver functions were used to detect discontinuity boundaries. For this purpose, Iterative deconvolution in time domain (Ligorria & Ammon, 1999) was used to calculate receiver functions, then, radial receiver functions were migrated to the depth according to the method proposed by Zhu (2000), to define seismic boundaries by Ps-converted phases along the seismic profile.

2. Geology and Tectonics

After the closure of the paleoTethys, the northern subduction of the NeoTethys begins, which caused the stretching of the Mesozoic back arc and the subsidence of the Cimmerian Mountain (Shojaat et al., 2003; Shafaii Moghadam & Stern, 2015). During the Paleogene period, the Iranian Plateau (especially in Eastern Iran) was dominated by tensile regimes, and this tension was probably associated with delamination and caused calc-alkaline magmatism in East Iran (Pang et al., 2013). In addition, the back-arc extension led to the rise and opening of several small-scale and short-term seas around the central-eastern subcontinent of Iran, such as the Sabzevar Ocean and the Sistan Ocean, which separated the central-eastern subcontinent of Iran from northeastern Iran and the Afghan block, respectively (Agard et al., 2006). These small seas were closed in the late Cretaceous-early Paleogene, which is probably responsible for the emplacement of the ophiolitic belts in the Sabzevar zone and the Sistan suture zone (Camp & Griffs, 1982; Saccani et al., 2010).

Rifting between the Afghan and Lut blocks, which started around Cenomanian time, create the Sistan Ocean that eroded during the late Paleocene, and the Sistan suture zone resulted from the collision between the Afghan and Lut blocks (Figure 1) (Tirrul et al., 1983). Subduction direction remains a controversial issue in this region (e.g.

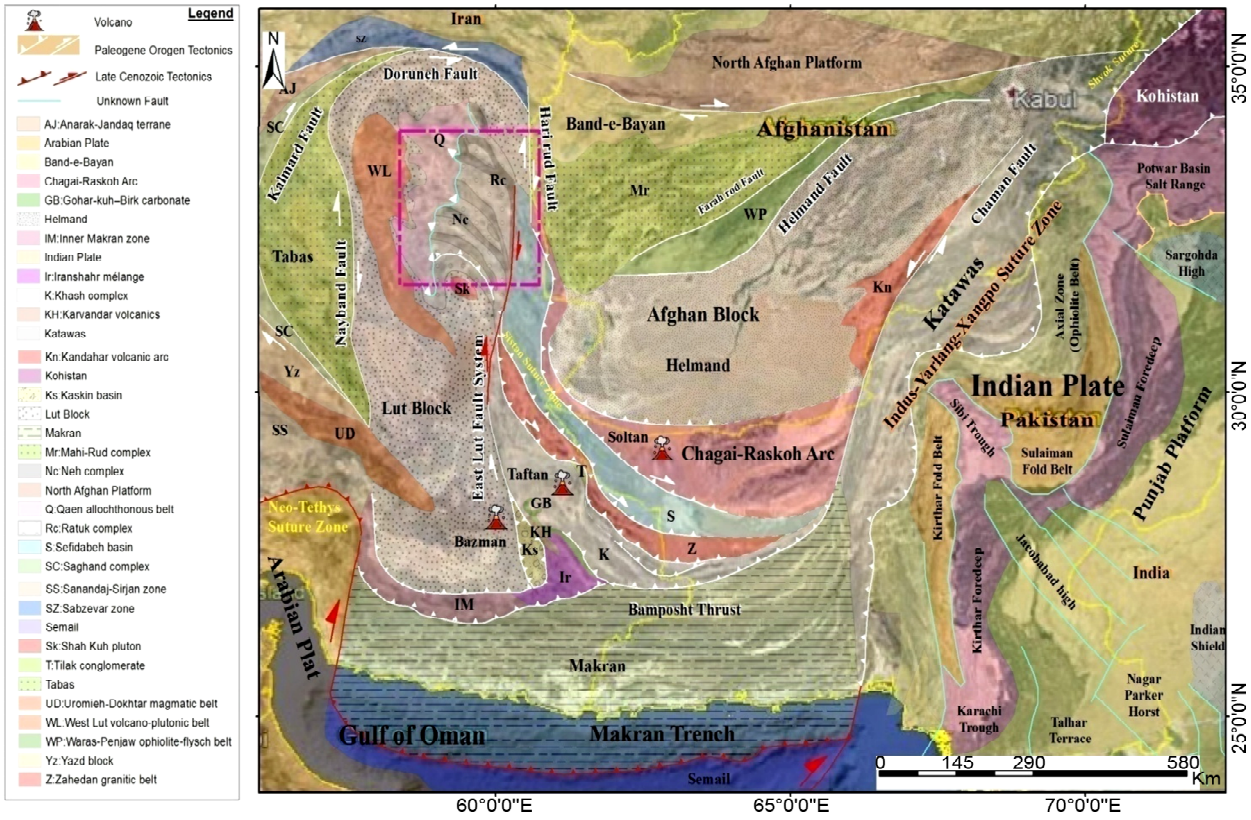

Figure 1. Map of stratigraphic-seismotectonic divisions and surface effects of major faults in eastern Iran, Afghanistan and the western part of the Indian plate. The map information is taken from Ahmad et al., 2012; Bagheri & Damani-Gol, 2020. The study area is marked with a bold pink box.

Fotoohi Rad et al., 2009; Bagheri & Damani Gol, 2020).

The collision of the Lut block with the Neh-Retuk accretionary-subduction complexes is marked by the end of marine sedimentation in the Middle Eocene and the beginning of significant folding in the Sefidabeh basin. Two related folding and transpression events have been revealed between the early Eocene and early Miocene times, and the third phase of metamorphism continued in the Miocene-Pliocene until the Quaternary, which can be recognized by the activity of right-lateral strike-slip faults with a north-northeast trend (Tirrul et al., 1983).

The main role of the faults in the east Iran is to provide the movement of the Lut Block towards the north with respect to the stable Afghan block (Walpersdorf et al., 2014). Igneous activities occurred in the Mesozoic and Cenozoic eras in Lut and Sistan regions, and the Mesozoic events are spatially limited to the strike-slip fault systems near the Retuk and Neh ophiolites, while the igneous events of the Cenozoic in Northern Lut are scattered and they can be related to the rise of asthenosphere due to delamination of the thickened lithosphere root by Afghan continental collision (Pang et al., 2013).

Stress field interactions on the Eastern Lut, including the Arabian-Eurasian oblique convergence, with a rate of about 22 mm per year (Vernant et al., 2004), the Makran subduction and the collision of the Indian plate with Eurasia, and the motion of the stable Afghan plate towards Iran, has caused the formation of the north-south strike-slip fault system. The collision of the Indian and Afghanistan plates with Eurasia has caused the counterclockwise rotation of the Lut Block relative to Eurasia (Soffel et al., 1996). Recently, Mattei et al. (2019) re-evaluated the rotation of the Lut Block and classified it into two groups, one is the clockwise rotation resulting from the action of the EW left-lateral strike-slip faults and the other is the anti-clockwise rotation resulting from the action of the NS right-lateral strike-slip faults.

GPS modeling and paleomagnetic results indicate that the crustal segments of the Central-Eastern Iranian subcontinent rotated in a horizontal plane from the Middle-Late Miocene, which probably played an important role in accommodation of the NS shortening (Mattei et al., 2019; Walpersdorf et al., 2014). GPS data indicates that the convergence towards the north in eastern Iran is accommodated by both 6-13 mm per year slip and counterclockwise rotation, 0.4±1°/Ma, of the Strike-slip fault systems (Walpersdorf et al., 2014).

3. Data and Methodology

In this study, the data recorded by 31 seismic stations were used to study the structure of the lower crust and the upper mantle of South Khorasan along the profile N39.61°E, with a length of about 230 km (Figure 2). These stations include two broadband stations belong to the International Institute of Earthquake Engineering and Seismology (IIEES), seven stations from the Institute of Geophysics, University of Tehran (IGUT), and 22 temporary seismic stations installed in South Khorasan in 2017 for nine months by IIEES (Figure 2 and Table 1). Teleseismic earthquakes with a magnitude greater than 5.5, which occurred at the

Table 1. Seismic station coordinates and their sensor types.

Station	Lat. (°N)	Long. (°E)	Elev. (m)	Institute	Sensor (Model)	Band	Maximum Period (s)
AFRZ	33.425	59.015	1497	IGUT	Trillium	MB	40
BAGH	32.7823	59.2048	2581	IGUT	SS1	SP	1
BAR	33.4256	59.9903	1711	IIEES	Lennartz	MB	20
BEN	33.304	59.8116	1938	IIEES	Lennartz	MB	20
BOQ	33.5175	60.0665	1028	IIEES	Lennartz	MB	20
BSRN	31.9651	59.1259	1416	BI	CMG-3T	BB	120
CHA	32.5533	59.4637	1890	IIEES	Guralp-6TD	SP	10
DAH	32.739	59.868	2341	IGUT	SS1	SP	1
DEH	32.1842	59.5197	1933	IIEES	Lennartz	MB	20
FER	32.6788	59.4528	2130	IIEES	Guralp_6TD	SP	10

Table 1. Continue.

Station	Lat. (°N)	Long. (°E)	Elev. (m)	Institute	Sensor (Model)	Band	Maximum Period (s)
GAZ	32.5971	59.3499	1760	IIEES	Guralp-6TD	SP	10
GHA	32.7358	59.1075	1927	IIEES	Lennartz	MB	20
GIV	32.5606	59.2504	1493	IIEES	Lennartz	MB	20
GOL	32.4002	59.6633	1875	IIEES	Guralp-6TD	SP	10
GUR	32.5389	59.6222	1925	IIEES	Guralp-6TD	SP	10
JIG	32.3089	59.5009	1860	IIEES	Guralp-6TD	SP	10
KOO	32.424	59.004	1940	IGUT	SS1	SP	1
MAH	32.7287	59.3856	2090	IIEES	Lennartz	MB	20
MAJ	32.5747	59.035	1449	IIEES	Lennartz	MB	20
MIA	32.4707	59.5235	1877	IIEES	Guralp-6TD	SP	10
MOK	32.4718	59.388	1512	IGUT	Guralp-6TD	SP	10
MON	33.192	59.667	2368	IGUT	SS1	SP	1
PEI	32.657	59.5903	1960	IIEES	Guralp-6TD	SP	10
ROB	32.7125	59.2833	2054	IIEES	Lennartz	MB	20
ROM	32.7047	59.2206	1872	IIEES	Lennartz	MB	20
SAL	32.644	59.2322	1638	IIEES	Lennartz	MB	20
SEI	33.0181	59.6206	2048	IIEES	Lennartz	MB	20
SHRT	33.6462	60.291	837	BI	CMG-3T	BB	100
SOL	32.8922	59.5136	1836	IIEES	Lennartz	MB	20
TEG	32.897	58.749	1745	IGUT	SS1	SP	20
ZOB	32.3908	59.7711	1833	IIEES	Lennartz	MB	20

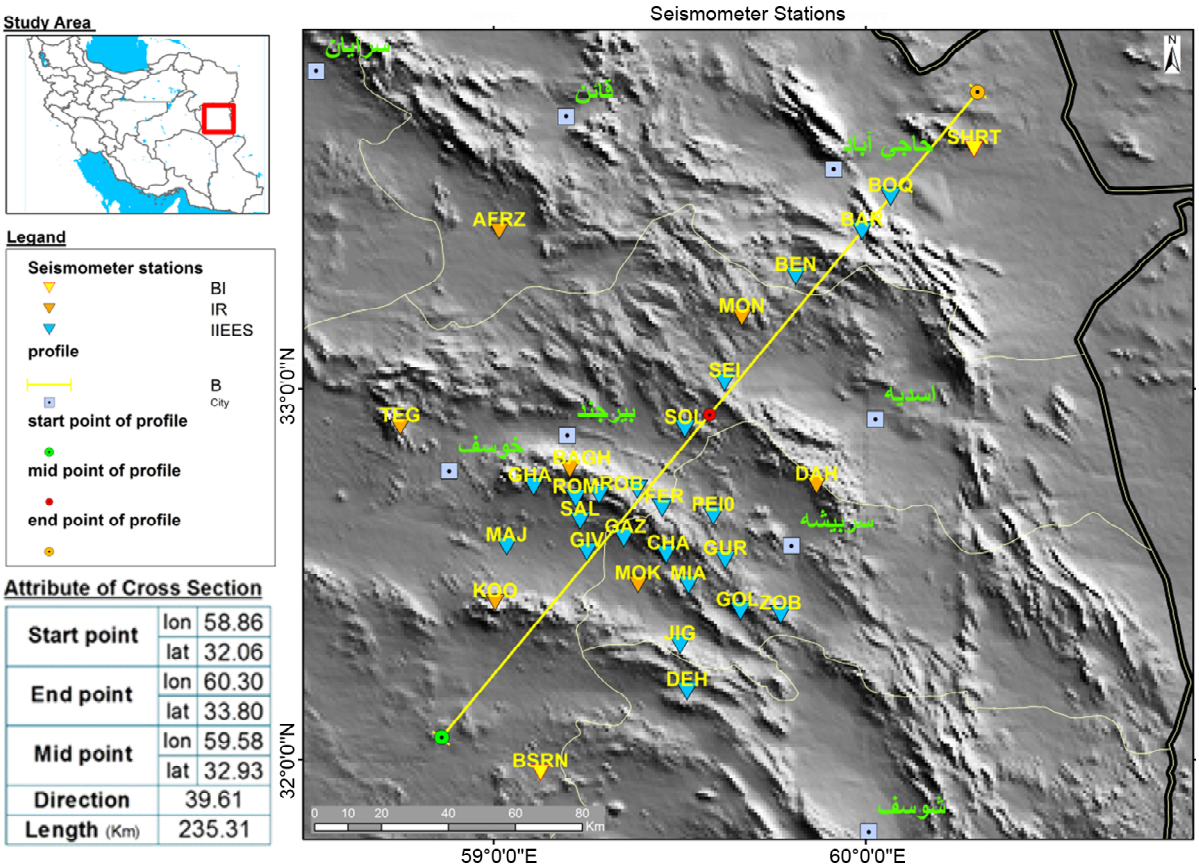

Figure 2. Location of two broadband stations of IIEES (yellow inverted triangle), seven stations belonging to the IGUT (inverted triangle in orange), and 22 temporary seismic stations installed by IIEES (inverted triangle in blue), located in South Khorasan (Eastern Iran). The northeast-southwest profile in this study is depicted with a yellow line.

epicentral distance between 30 and 90 degrees, were selected to calculate the P receiver functions (Figure 3).

Ps converted phase is observed in the radial component, thus the seismogram components are transferred from ZNE to ZRT coordinate system as represented in Figure (4) for station SHRT. To ensure the quality of our data, we applied a selection criterion that excluded seismograms with a signal-to-noise ratio of less than two. This approach allowed us to focus on high-quality data, which are essential for accurate analysis and interpretation

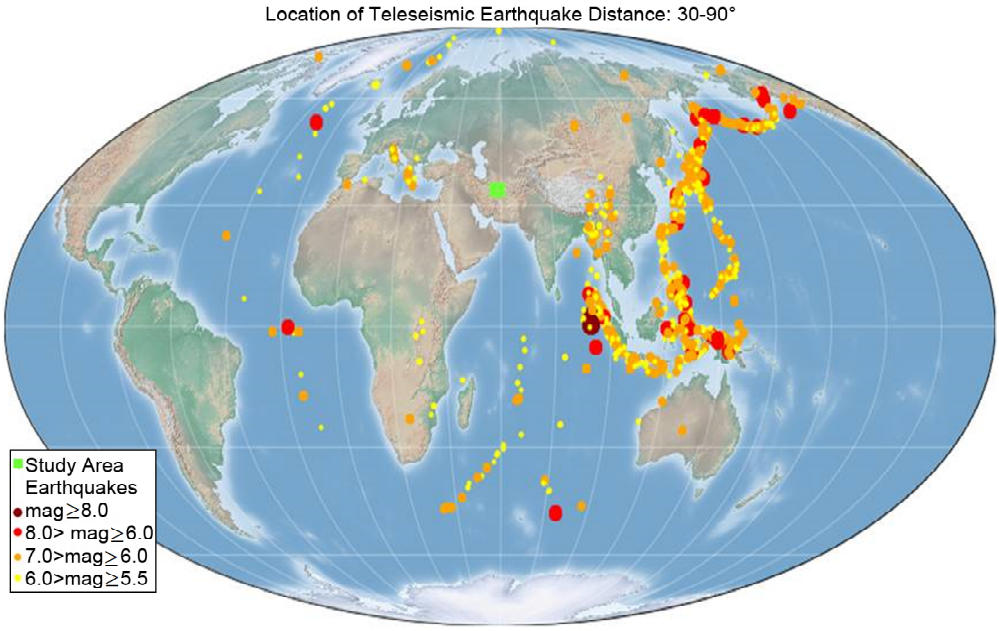

Figure 3. The epicenter of earthquakes with a magnitude greater than 5.5, occurred at epicentral distance between 30o and 90o relative to the study area (green square).

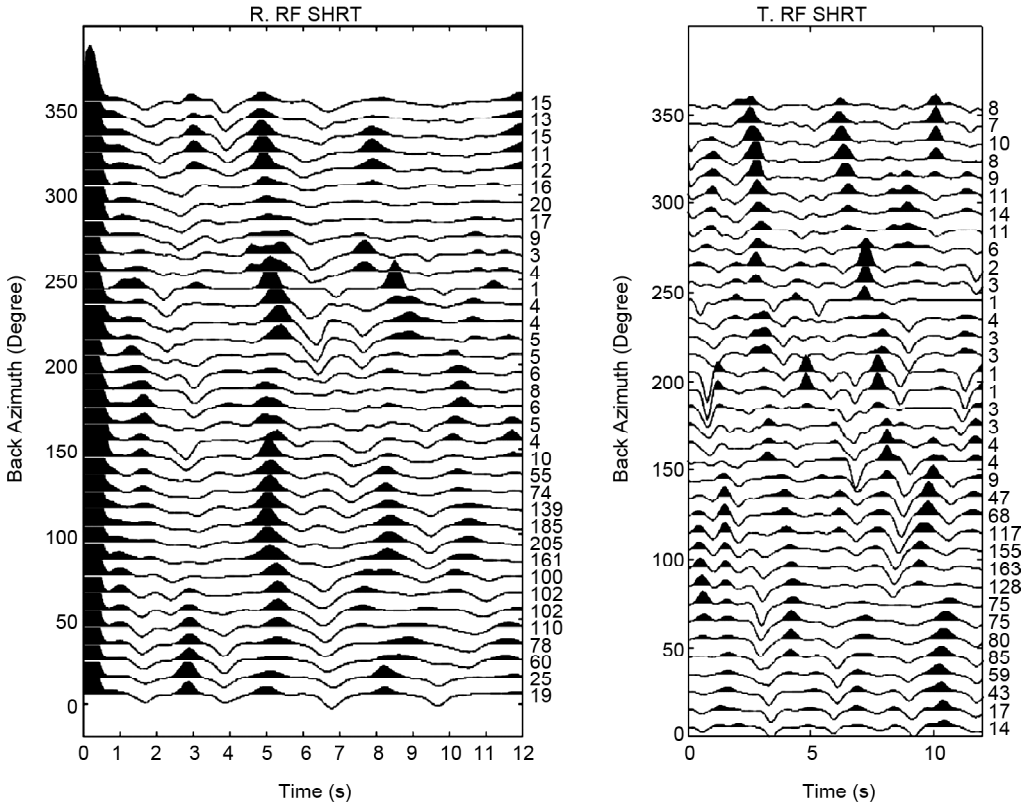

Figure 4. Radial and transverse receiver functions for SHRT station stacked for back-azimuth distances in 10-degree bins. A coherent positive amplitude is observed in the radial component around 5 s, which may indicate the Ps Moho converted phase.

of seismic signals. The initial time window for calculating P receiver functions was considered from 60 s before and 120 s after the onset of the P wave. The P receiver functions were calculated by deconvolution of the vertical component from the radial component in the time domain using an iterative time domain deconvolution method (Kikuchi & Kanamori, 1982, Ligorria & Ammon, 1999). Deconvolution operation removes the instrument response, the source and path effects. The receiver functions have high frequency noises in the time domain. To eliminate them, a Gaussian low-pass filter with a width of 1 Hz and Gaussian coefficient of 5 was applied.

The receiver functions calculated in the final step are checked visually, and receiver functions with negative amplitudes at zero were dropped from the data set. In addition, receiver functions with Moho Ps conversions around 5 s and their shape consistent with the dominant shape of other receiver functions at the same station are selected. Receiver functions represent subsurface structures and sample a specific spatial distance. In order to find the piercing point of the P wave rays at the Moho depth (~40 km), the ray parameter of the P phase was calculated. Figure (5) represents the piercing points of the P receiver functions at 40 km depth. They indicate that many rays were received from the east.

A total number of 1775 (out of 2347) receiver functions were selected and migrated for the stations located 20 km from the profile. The common conversion point (CCP) stacking method (Zhu, 2000) was used to image the structure of the crust and the upper mantle along the profile. In this method, in order to migrate the receiver functions, the ray path of each receiver function is calculated through the IASP91 velocity model, and the receiver function is placed on its related ray path. Therefore, the Ps converted phase is placed on the actual location where the P to S conversion took place. Then, a 3D grid is constructed and the average of the amplitudes in each bin is calculated and projected on the profile (Figure 6). Figure (6) shows the amplitude stacking of common conversion points on the profile. The dimensions of the bins in this image are 10 km, 4 km and 2 km in x, y and z directions, respectively. This selection of parameters gives us a smoothed image of the structural variations across the region. In order to retain the highest-possible spatial resolution, smoothing was minimized in the construction of the images, and the depth profile is divided into grids with spacing of 2 km along the profile and 2 km in depth. Therefore, we observe the details and can follow the trend of the discontinuities (Figure 6).

4. Results and Discussions

The details of the crust and upper mantle have not been accurately determined in Eastern Iran due to the lack of seismic data. However, a few large-scale studies have been conducted recently. For example, Nasrabadi et al. (2019) studied the Moho depth changes in Central and Eastern Iran and reported a decrease in crustal thickness in

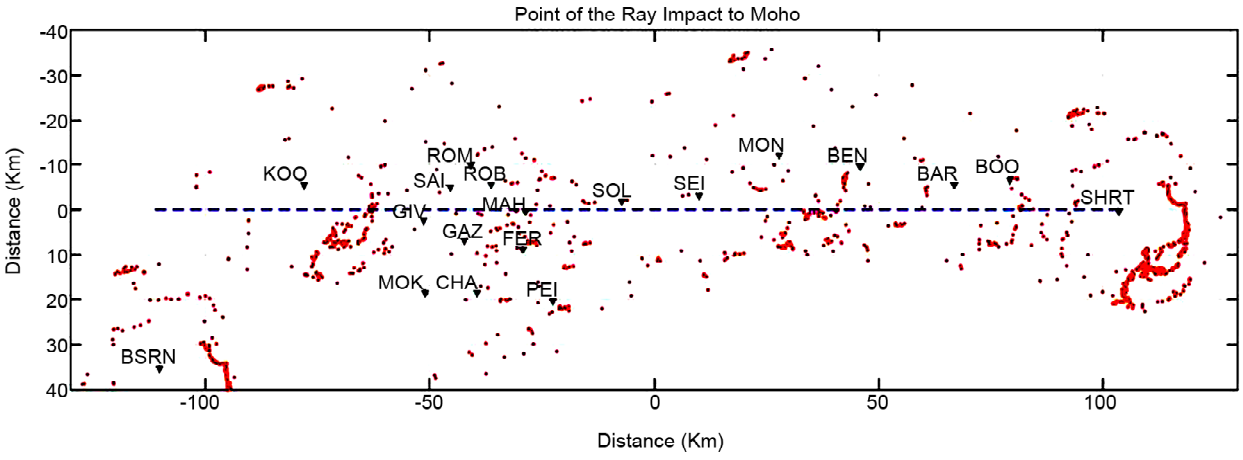

Figure 5. The black inverted triangle indicates the location of the seismic stations and the red dots indicate the piercing points of teleseismic P phase at a depth of 40 km.

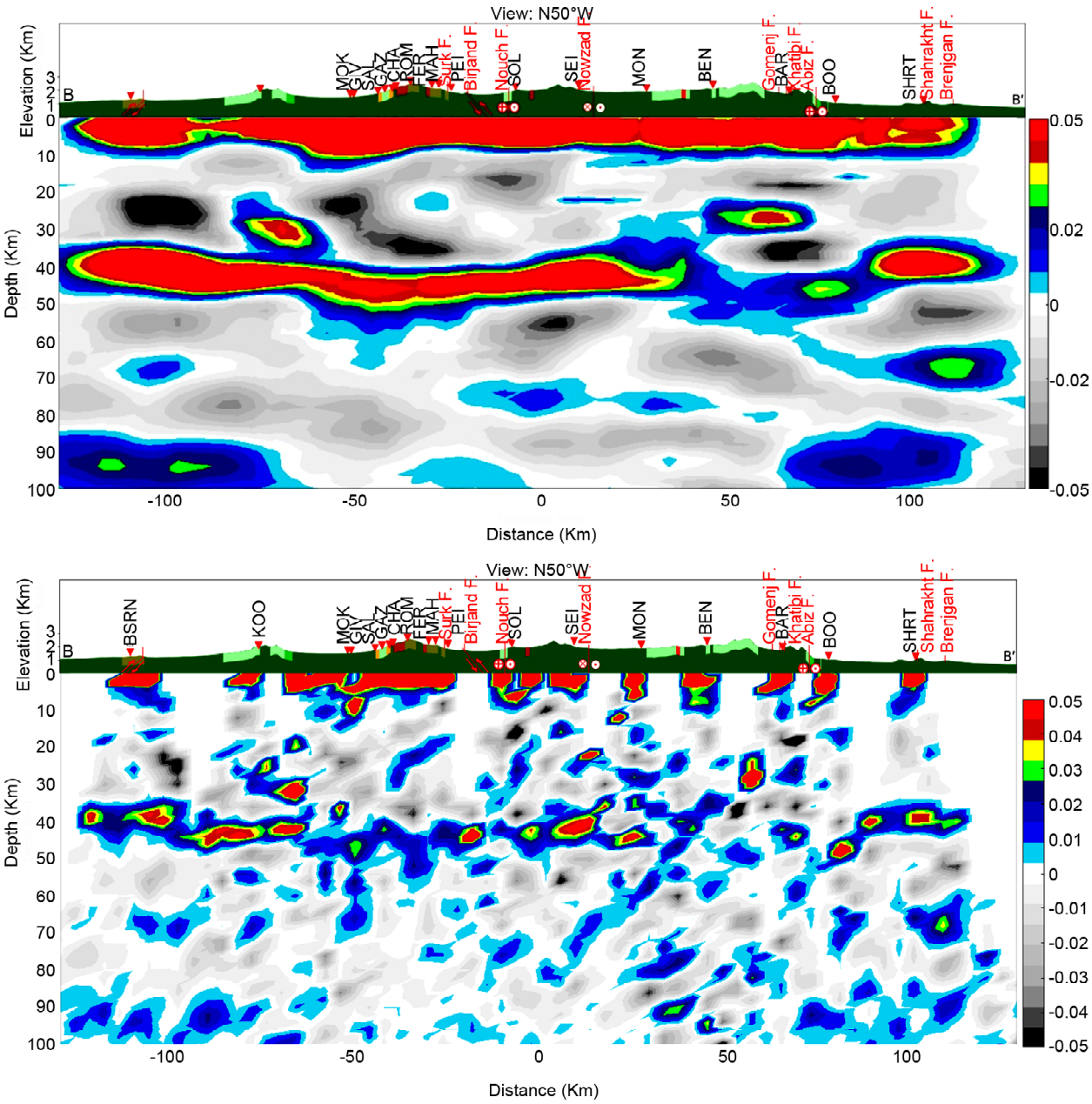

Figure 6. Migration of receiver functions obtained by two different smoothing parameters.

Eastern Iran to 38 km. They related thin crust to the presence of major strike faults and the low shortening rate in Eastern Iran as noted by Vernant et al. (2004) and Khorrami et al. (2019). Moreover, Movaghari & Javan-Doloei (2020) have derived the 3D shear wave velocity (Vs) model of the crust and uppermost mantle under Iran plateau using phase velocity ambient noise tomography and proposed a low crustal thickness beneath eastern part of Iran in comparison to the thick crust of Central Iran. Simultaneous inversion of the P-wave receiver functions and Rayleigh wave group velocity shows thin lithosphere and a 40 km thick crust under the Lut block (Namvaran et al., 2020). Wu et al. (2020) studied the lithosphere and asthenosphere in the northeast to the east of the Iran plateau by studying S wave receiver functions. They observed a shallow Moho (about 45 km) and a relatively flat lithosphere-asthenosphere boundary under eastern Iran at a depth of 80-90 km. Kaviani et al. (2020) obtained the 3D shear wave velocity (Vs) model of the uppermost mantle and lower crust of the Middle East using Rayleigh waves from ambient noise and regional earthquakes. Their 3D velocity model shows the low-velocity upper mantle under the Lut block too, which may indicate hotter material compared to the surrounding areas. Movaghari

et al. (2021) revised 3D shear wave velocity model beneath the Iranian plateau and once again presented a thin crust for eastern part of Iran. Therefore, recent regional studies in Iran plateau proposed a thin crust in eastern part of Iran (Motaghi et al., 2012a, 2012b, 2015).

The most prominent P-S conversion in the image obtained by depth migration of receiver functions indicate the Moho boundary at a depth of 40 km, which is flat in most parts of the profile (Figure 6). Other studies have also reported the Moho discontinuity at about 40 km (e.g. Motaghi et al., 2012a,b, 2015; Entezar-Saadat et al., 2017; Nasrabadi et al., 2019; Movaghari & Javan Doloei, 2020; Namvaran et al., 2020; Wu et al., 2020; Kaviani et al., 2020; Movaghari et al., 2021).

The CCP image of the present study clarifies the presence and geometry of the discontinuity boundaries in the crust and upper mantle in more details (Figure 6). The most important feature in this image is the Moho boundary offset below the BAR, BEN and BOQ stations, at a distance of 40 to 90 km from the center of the profile, beneath Lut and Afghan blocks boundary. There is a clear boundary at a depth of about 30 km. This boundary is beneath major NS strike-slip faults that accommodate some part of the Eastern Iran motion relative to the Afghan block to the north. A less smoothed image also shows a complex structure in this region and an apparent dip toward the southwest continues to the deeper parts in the upper mantle.

Another crustal boundary can be seen at a distance of -70 km from the center of the profile and at a depth of about 28 km (Figure 6) that is located under Basiran (BSRN) and Koh-Shah (KOO) stations, showing a low-angle dip towards the north-east.

Some reverse faults in the northern part of the Sistan suture are considered as the termination of the major north-south strike-slip faults (Walker & Khatib, 2006). They are also considered as a result of wedge confining pressure in this region (Baniadam et al., 2019). Moreover, it is possible to observe major low-angle fault in the suture zone that can affect the entire crust and causes thickening of the crust (e.g. Motaghi et al., 2017). However, the direction of subduction in this area is still unclear (e.g. Tirrul et al., 1983; Zarrinkoub et al., 2012) and if we accept that the subduction slope in this area was towards the west, the thickening of the crust in this area under the studied profile may be probable. Of course, it should be considered that the studied profile is in the northeast direction, and the slight thickenings observed in this study cannot represent the actual amount of thickening due to the possible mentioned mechanism. However, assuming westward subduction, the observed crust thickening is less compared to Zagros, which can be related to the significant role of strike-slip faults in the shortening by their rotation and/or contribution in the extrusion of the fault-bounded crustal blocks (e.g. Walker & Jackson, 2004; Walpersdorf et al., 2014; Baniadam et al., 2019).

5. Conclusion

`P receiver function analysis is one of the most effective tools to obtain a robust image along with the desired profiles. Taking advantage of the 31 seismic stations from different networks within Lut Block, a valuable and specific large dataset of teleseismic waveforms was assembled. The results obtained from receiver functions analysis and depth migration image (CCP) along NE studied profile can be summarized as follows. Ps converted waves on receiver functions can be observed at about 5 s from direct wave that indicates the Moho boundary, which is approximately flat along a 230 km NE profile. This boundary shows a small increase in depth at distances of 40 to 90 km (beneath the Afghan-Lut border) and -40 to -60 km (beneath Bagheran Mountain) from the center of the profile. It implies a relatively thin crust beneath the Afghan and Eastern Iran collision zone where strike-slip motion has a significant role in the deformation of Eastern Iran.

Acknowledgement

This work and related field study are supported by the International Institute of Earthquake Engineering and Seismology (IIEES) under project number 672. We warmly thank Dr. Khalil Motaghi and Dr. Saeed Soltani Moghadam for their constructive comments in reviewing the paper. We appreciate the Institute of Geophysics,

University of Tehran (IGUT) and the Iranian Seismological Center (IRSC) for providing permanent station data. Special thanks to Dr. Ali Moradi and Ali Hashemi Gazar as well as Birjand Seismic Network staff for their hospitality during the field study. We also appreciate the kind people of South Khorasan province who cooperated to provide suitable locations to install the temporary seismic stations. Special thanks also goes to our IIEES field team colleagues participating in seismic station installation and data collection in harsh conditions.

References

Agard, P., Monie, P., Gerber, W., Omrani, J., Molinaro, M., Meyer, B., Labrousse, L., Vrielynck, B., Jolivet, L., & Yamato, P. (2006). Transient, syn-obduction exhumation of Zagros blueschists inferred from P-T-deformation-time and kinematic constraints: implications for Neotethyan wedge dynamics. *J. Geophys. Res.*, *111*, B11401, http://dx.doi.org/10.1029/2005JB004103.

Ahmad, A., Ali, M., Baitu. A.H., & Sardar, N. (2012). *Tectono-Stratigraphic Model for Ghazij Formation in Kirthar Foldbelt, Pakistan*. Poster presentation at AAPG International Convention and Exhibition, Singapore, 16-19.

Allen, M.B., Kheirkhah, M., Emami, M.H., & Jones, S.J. (2011). Right-lateral shear across Iran and kinematic change in the Arabia-Eurasia collision zone. Geophys. *J. Int.*, *184*(2), 555-574, http://doi:10.1111/j.1365-246x.2010.04874.x.

Bagheri, S., Damani Gol, Sh. (2020). The Eastern Iranian Orocline. Earth-Science Reviews, 210, 103322. doi:10.1016/j.earscirev.2020.103322.

Bagheri, S., & Stampfli, G.M. (2008). The Anarak, Jandaq and Posht-e-Badam metamorphic complexes in Central Iran: New geological data, relationships and tectonic implications. *Tectonophysics*, *451*, 123-155, https://doi.org/10.1016/j.tecto.2007.11.047.

Baniadam, F., Shabanian, E., & Olivier, B. (2019). The kinematics of the Dasht-e Bayaz earthquake fault during Pliocene-Quaternary: Implications for the tectonics of eastern Central Iran. *Tectonophysics*, *772*, 228218, https://doi.org/10.1016/j.tecto.2019.228218.

Berberian, M., & King, G.C.P. (1981). Towards a paleogeography and tectonic evolution of Iran. *Canadian Journal of Earth Sciences*, *18*(2), 210-265, https://doi.org/10.1139/e81-019.

Camp, V.E., & Griffis, R.J. (1982). Character, genesis and tectonic setting of igneous rocks in the Sistan suture zone, eastern Iran. *Lithos*, *15*, 221-239.

Entezar-Saadat, V., Motavalli-Anbaran, S.H., & Zeyen, H. (2017). Lithospheric structure of the Eastern Iranian plateau from integrated geophysical modeling: a transect from Makran to the Turan platform. *J. Asian Earth Sci.*, *138*, 357-366, http://dx.doi.org/10.1016/j.jseaes.2017.02.024.

Fotoohi Rad, G.R., Droop, G.T.R., & Burgess, R. (2009). Early cretaceous exhumation of high pressure metamorphic rocks of the Sistan Suture Zone, eastern Iran. *Geol. J.*, *44*, 104-116, https://doi.org/10.1002/gj.1135.

Hollingsworth, J., Fattahi, M., Walker, R.T., Talebian, M., Bahroudi, A., Bolourchi, M., Jackson, J.A., & Copley, A. (2010). Oroclinal bending, distributed thrust and strike-slip faulting, and the accommodation of Arabia-Eurasia convergence in NE Iran since the Oligocene. *Geophys. J. Int.*, *181*, 1214-1246.

Kaviani, A., Paul, Ann., Moradi, A., Mai, P.M., Pilia, S., Boschi, L., Rumpker, G., Lu, Y., Tang, Z., & Sandvol, E. (2020). Crustal and uppermost mantle shear-wave velocity structure beneath the Middle East from surface-wave tomography. *Geophysical Journal International*, *221*(2), 1349-1365, doi: 10.1093/gji/ggaa075.

Khorrami, F., Vernant, Ph., Masson, F., et al. (2019). An up-to-date crustal deformation map of Iran using integrated campaign-mode and permanent GPS velocities. *Geophys. J. Int.*, *217*, 832-843, doi: 10.1093/gji/ggz045.

Kikuchi, M., & Kanamori., H. (1982). Inversion of complex body waves. *Bull. Seism. Soc. Am.*, *72*, 491-506.

Ligorria, J.P., & Ammon, C.J. (1999). Iterative deconvolution and receiver-function estimation. *Bull. Seismol. Soc. Am.*, *89*, 1395-1400.

Mattei, M., Cifelli, F., Alimohammadian, H., & Rashid, H. (2019). The role of active strike-slip faults and opposite vertical axis rotations in accommodating eurasia-arabia shortening in Central Iran. *Tectonophysics*, *774*, 28243, http://doi:10.1016/j.tecto.2019.228243.

Movaghari, R., & Javan Doloei, G. (2020). 3-D crustal structure of the Iran plateau using phase velocity ambient noise tomography. *Geophys. J. Int.*, *220*(3), 1555-1568, https://doi.org/10.1093/gji/ggz537.

Movaghari, R., JavanDoloei, G., Yang, Y., Tatar, M., & Sadidkhouy, A. (2021). Crustal radial anisotropy of the Iran plateau inferred from ambient noise tomography. *Journal of Geophysical Research*, *126*(4), https://doi.org/10.1029/2020JB020236.

Motaghi, K., Tatar, M., & Priestley, K. (2012a). Crustal thickness variation across the northeast Iran continental collision zone from teleseismic converted waves. *Journal of Seismology*, *16*, 253-260.

Motaghi, K., Tatar, M., Shomali, Z.H., Kaviani, A., & Priestley, K. (2012b). High resolution image of uppermost mantle beneath NE Iran continental collision zone. *Physics of the Earth and Planetary Interiors*, *208*, 38-49.

Motaghi, K., Tatar, M., Priestley, K., Romanelli, F., Doglioni, C., & Panza, G.F. (2015). The deep structure of the Iranian Plateau. *Gondwana Research*, *28*(1), 407-418.

Motaghi, K., Shabanian, E., & Kalvandi, F. (2017). Underplating along the northern portion of the Zagros suture zone, Iran. *Geophys. J. Int.*, *210*(1), 375-389.

Namvaran, M., Tatar, M., & Motavalli-Anbaran, S.H. (2020). Imaging the 2-D crust and upper mantle structure of the Iranian plateau resolved by potential field and seismic data. *Physics of the Earth and Planetary Interiors, 300*, 106445, https://doi.org/10.1016/j.pepi.2020.106445.

Nasrabadi, A., Sepahvand, M.R., & Dadjo, Z. (2019). Moho depth variations and Vp/Vs ratios in the seismotectonic zones of Central Iran, Eastern Iran, and Makran: using a modified Zhu and Kanamori method. *Journal of Seismology*, *23*, 839-851, https://doi.org/10.1007/s10950-019-09837-y.

Nozaem, R., Mohajjel, M., Rossetti, F., Della Seta, M., Vignaroli, G., Yassaghi, A., Salvini, F., & Eliassi, M. (2013). Post-Neogene right-lateral strike-slip tectonics at the north-western edge of the Lut Block (Kuh-e-Sarhangi Fault), Central Iran. *Tectonophysics*, *589*, 220-233, doi:10.1016/j.tecto.2013.01.001.

Pang, K.N., Chung, S.L., Zarrinkoub, M.H., Khatib, M.M., Mohammadi, S.S., Chiu, H.Y., Chu, C.H., Lee, H.Y., & Lo, C.H. (2013). Eocene-Oligocene post-collisional magmatism in the Lut-Sistan region, eastern Iran: Magma genesis and tectonic implications. Lithos., 180-181, 234-251, https://doi.org/10.1016/j.lithos.2013.05.009.

Saccani, E., Delavari, M., Beccaluva, L., & Amini, S. (2010). Petrological and geochemical constraints on the origin of the Nehbandan ophiolitic complex (eastern Iran): Implication for the evolution of the Sistan Ocean. *Lithos.*, https://doi.org/10.1016/j.lithos.2010.02.016.

Shafaii Moghadam, H., & Stern, R.J. (2015). Ophiolites of Iran: Keys to understanding the tectonic evolution of SW Asia: (II) Mesozoic ophiolites. *Journal of Asian Earth Sciences*, *100*, 31-59, doi:10.1016/j.jseaes.2014.12.016.

Shojaat, B., Hassanipak, A.A., Mobasher, K., & Ghazi, A.M. (2003). Petrology, geochemistry and tectonics of the Sabzevar ophiolite, north central Iran. *Asian Earth Sci.*, *21*, 1053-1067.

Soffel, H.C., Schmidt, S., Davoudzadeh, M., & Rolf, C. (1996). New palaeomagnetic data from Central Iran and a Triassic palaeoreconstruction. *Geol. Rundsch.*, *85*(2), 293-302.

Stocklin, J. (1968). Structural history and tectonics of Iran: a review. *Am. Ass. Petrol. Geol. Bull.*, *52*, 1229-1258.

Tirrul, R., Bell, I.R., Griffis, R.J., & Camp, V.E. (1983). The Sistan suture zone of eastern Iran. *Geol. Soc. Am. Bull.*, *94*, 134.

Vernant, Ph., Nilforoushan, F., Hatzfeld, D., Abbassi,

M.R., Vigny, C., Masson, F., Nankali, H., Martinod, J., Ashtiani, A., Bayer, R., Tavakoli, F., & Chéry, J. (2004). Present-day crustal deformation and plate kinematics in the Middle East constrained by GPS measurements in Iran and northern Oman. *Geophys. J. Int.*, *157*(1), 381-398, http://doi:10.1111/j.1365-246x.2004.02222.x.

Walker, R., & Jackson, J. (2004). Active tectonics and late Cenozoic strain distribution in central and eastern Iran, *Tectonics*, *23*, TC5010, DOI:10.1029/2003TC001529.

Walker, R.T., & Khatib M.M. (2006). Active faulting in the Birjand region of NE Iran. *Tectonics*, *25*, TC4016, DOI:10.1029/2005TC001871.

Walpersdorf, A., Manighetti, I., Mousavi, Z., Tavakoli, F., Vergnolle, M., Jadidi, A., Hatzfeld, D., Aghamohammadi, A., Bigot, A., Djamour, Y., Nankali, H., & Sedighi, M. (2014). Present-day kinematics and fault slip rates in eastern Iran, derived from 11 years of GPS data. *Journal of Geophysical Research: Solid Earth*, *119*(2), 1359-1383, Doi:10.1002/2013JB010620.

Wu, Z., Chen, L., Talebian, M., Wang, X., Jiang, M., Ai, Y., Lan, H., Gao, Y., Khatib, M.M., Hou, G., Chung, S.L., Liang, X., Zhao, L., Naimi Ghassabian, N., Xiao, W., & Zhu, R. (2020). Lateral structural variation of the lithosphere-asthenosphere system in the northeastern to eastern Iranian plateau and its tectonic implications. *Journal of Geophysical Research: Solid Earth*, http://doi:10.1029/2020JB020256.

Zarrinkoub, M.H., Pang, K.N., Chung, S.L., Khatib, M.M., Mohammadi, S.S., Chiu, H.Y., & Lee, H.Y. (2012). Zircon U\Pb age and geochemical constraints on the origin of the Birjand ophiolite, Sistan suture zone, eastern Iran. *Lithos*, *154*, 392-405.

Zhu, L. (2000). Crustal structure across the San Andreas Fault, southern California from teleseismic converted waves. *Earth and Planetary Science Letters*, *179*(1), 0-190, Doi:10.1016/s0012-821x(00)00101-1.